Journal of the Korean Nuclear Society
Volume 30, Number 5, pp.452~461, October 1998

Pin Power Distribution Determined by Analyzing the Rotational Gamma Scanning Data of HANARO Fuel Bundle

Jae Yun Lee and Hee Dong Choi
Seoul National University
San 56-1, Shinlim-dong, Kwanak-gu, Seoul 151-742, Korea

(Received March 10, 1998)

Abstract

The pin power distribution is determined by analyzing the rotational gamma scanning data for 36 element fuel bundle of HANARO. A fission monitor of Nb^{95} is chosen by considering the criteria of the half-life, fission yield, emitting γ-ray energy and probability. The γ-ray spectra were measured in Korea Atomic Energy Research Institute(KAERI) by using a HPGe detector and by rotating the fuel bundle at steps of 10°. The counting rates of Nb^{95} 766 keV γ-rays are determined by analyzing the full absorption peak in the spectra. A 36×36 response matrix is obtained from calculating the contribution of each rod at every scanning angle by assuming 2-dimensional and parallel beam approximations for the measuring geometry. In terms of the measured counting rates and the calculated response matrix, an inverse problem is set up for the unknown distribution of activity concentrations of pins. To select a suitable solving method, the performances of three direct methods and the iterative least-square method are tested by solving simulation examples. The final solution is obtained by using the iterative least-square method that shows a good stability. The influences of detection error, step size of rotation and the collimator width are discussed on the accuracy of the numerical solution. Hence an improvement in the accuracy of the solution is proposed by reducing the collimator width of the scanning arrangement.

1. Introduction

The gamma scanning as a method of nondestructive assay was adopted on monitoring of post-irradiated fuel by Butterfield and Davies in 1971 and now settled as one of the standard monitoring methods[1,2]. It is used in monitoring of the axial burnup or the power distribution of fuels and the distribution of fission products in fuel cross section. The application of 2-dimensional(2-D) monitoring, so-called tomography, to the image reconstructions has been established in a diverse field of electron micrography, medical diagnostics and astrophysics while the similarity of their mathematical foundation lets a close connection for interdisciplinary research[3-5]. The method has been used in the field of nuclear engineering for studying the migration of fission products within

fuel element but active applications were reported recently for monitoring the contents of radiowaste container[6-10]. If a reliable method is established for 2-D monitoring the power distribution of pins by scanning the fuel bundle, it will save the efforts of the scan after disassembling and also providing core diagnostics and safety analysis with real set of experimental data. Hence the aim of this study is seeking a method of determining the pin power distribution from bundle scanning data instead of time-consuming individual rod scanning after disassembling. The method tried in this study is applied to obtain the pin power distribution of HANARO fuel bundle.

The 2-D gamma scanning is comprised of the measurement procedures, analysis of data, determining the response matrix and solving the inverse problem. In a typical fuel rod monitoring, the fuel bundle is scanned in transversal direction at several viewing angles and with a narrow collimator. In such case, however, the required number of measurement is large and hence the big size of inverse problem amplifies the numerical errors to result in unreliable quantitative solution. Therefore in the present study, a 36 rotational scan dataset for the fuel bundle is used to reduce the size of response matrix and to seek the possibility of quantitative analysis.

Fig. 1 shows the scanning geometry for the data used in this work. For the counting rate M_θ with the bundle rotated to angle θ, a linear equation is given by

$$M_\theta = R_{\theta,1}S_1 + R_{\theta,2}S_2 + \cdots + R_{\theta,36}S_{36} \quad (\theta = 0°, \cdots, 350°) \tag{1}$$

where $R_{\theta,i}$ is the response to a unit source density of the i-th rod for the scan at angle of θ and S_i is the source density of the i-th rod. The counting rate vector M is obtained by analyzing the measured spectra, and the 36×36 response matrix is calculated theoretically giving the

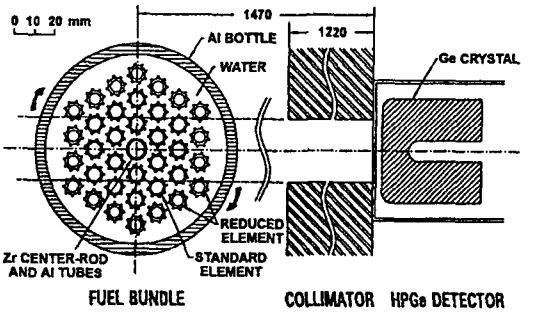

Fig. 1. A Cross Sectional View of the Gamma Scanning Arrangement.

following inverse problem for the unknown vector $S(S_1, \cdots, S_{36})$,

$$M = \mathbf{R}S. \tag{2}$$

The eq. (2), however, falls under ill-posed problem due to the statistical error of detection and the intrinsic error in calculating the response. Hence to get a stable solution the selection of an appropriate solving method is required. In this work, the iterative least-square method is chosen from the performance test and comparison with several direct methods. The pin power distribution, therefore, is determined by applying this method and is compared with the calculated result which had been performed in KAERI[11] by using the MCNP code. In addition, the sensitivity of the solution's accuracy is analyzed to get how it is dependent on factors related to the measurement such as the width of collimator, the statistical error of counting and the step size of rotation.

2. Analysis

2.1. Fission Monitor

The criteria for fission monitor of fuel power are

Table 1. The Main Fission Products and the Relevant Physical Data[14,15].

Characteristics \ Nuclide	Zr/Nb-95		Cs-137	Ru-103
Half Life	64.02 d/34.975 d		30.07yr	39.26 d
Accumulated Fission Yield [#/Fission] (from U-235 at 0.0235eV)	$6.50/6.49\times10^{-2}$		6.27×10^{-2}	3.03×10^{-2}
Neutron absorption Cross Section (Fission Spectrum Averaged)	0.0387 b/ 0.0718 b		0.0099 b	0.049 b
γ-Ray Energy [keV]	Zr	Nb		
(Emission Probability [%])	724.20 (43.1)	765.79 (99.8)	661.66 (85.0)	497.08 (90.9)
	756.73 (54.6)			

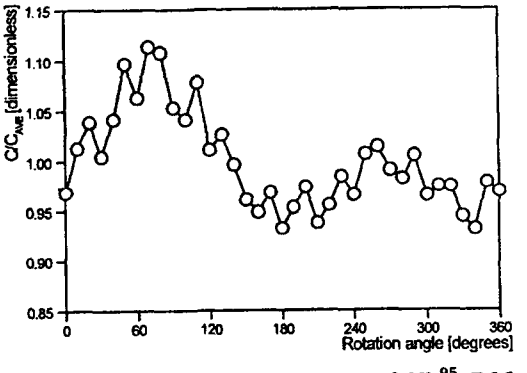

Fig. 2. Measured Counting Rates of Nb^{95} 766 keV γ-rays Obtained from the Rotational Scanning.

1) shorter half-life, 2) higher fission yield, 3) smaller cross section of neutron absorption, 4) higher γ-ray energy and emission probability, and 5) less migration from the produced position[1,12]. The irradiation time of ca 17 hrs for the present fuel makes the item 1) unconcerned. The items 2) and 4) are to reduce the statistics of data reliable by the high counting rate. With regard to the criterion 5), Cs^{137} only is known to have a considerable migration even though it is negligible under the burning temperature lower than 1100 °C[1,3,4]. In case of the present fuel, the burning temperature was kept about 100 °C[13] hence the criterion 5) is irrelevant. The main fission products and the relevant physical data for choosing the fission monitor are listed in Table 1. The 766 keV γ-rays from Nb^{95} give far higher counting rate than others and satisfy all the above criteria except the criterion 3). The neutron absorption cross section of Nb^{95} is relatively large, but still the loss from neutron absorption is negligible since the neutron flux is around $10^{12}\sim10^{14}$ neutrons/cm^2 · sec in HANARO. One thing to concern is that Nb^{95} is the decay product from Zr^{95}. It was 345 days after the irradiation when the fuel bundle had been scanned. Hence a transient equilibrium was established between their activities to give a proportionality between the fuel power and the activity concentration of Nb^{95}. Fortunately, the intervening production of Nb^{95} by the activation and decay of Zr center rod is reported to be negligible judging from an axial scanning measurement[11]. Therefore Nb^{95} 766 keV γ-rays are chosen as fission monitor.

The 36 γ-ray spectra measured and supplied by KAERI are analyzed with HYPERMET

program[16] to obtain accurate peak areas. The determined counting rate of full absorption peak for Nb^{95} 766 keV γ-rays is shown in Fig. 2. In the figure, the statistical errors of data are within 0.7 % and smaller than the symbol size. The data are shown in normalization to the average counting rate C_{AVE}.

2.2. Response Matrix

The elements of response matrix are calculated for the unit activity concentration of each fuel pin and for each rotational direction of the bundle. The solid angle of the γ-ray source, the self-attenuation in the fuel meat and the attenuations in the medium on the path of γ-rays to the detector have been considered in the theoretical calculation of response. The differential counting rate dM [cps] for γ-rays of a particular energy and originating from an infinitesimal volume $d\mathbf{r}_s$ of the fuel is given by[6,17]

$$dM = pS(\mathbf{r}_s)d\mathbf{r}_s \int_{A_d} d\Omega(\mathbf{r}_s, \mathbf{r}_d) \exp\left[-\sum_k \mu_k d_k(\mathbf{r}_s, \mathbf{r}_d)\right] \varepsilon'(\mathbf{r}_s, \mathbf{r}_d) \quad (3)$$

where p : emission probability [γ-rays/Bq],
S : activity concentration [Bq/mm^3],
$\mathbf{r}_s$: position vector of the infinitesimal volume source,
$\mathbf{r}_d$: vector of the entering position on the detector surface,
$d\Omega$: differential solid angle for the infinitesimal area of detector surface,
μ_k: linear attenuation coefficient of the k-th medium [mm^{-1}],
$d_k(\mathbf{r}_s,\mathbf{r}_d)$: the path length in the k-th medium for the γ-rays entering $\mathbf{r}_d$ and emitted from $\mathbf{r}_s$ [mm],
$\varepsilon'(\mathbf{r}_s,\mathbf{r}_d)$: full absorption peak efficiency for the γ-rays entering $\mathbf{r}_d$ and emitted from $\mathbf{r}_s$ [dimensionless].

Here the attenuation effects in the medium include the self-attenuation in the fuel meat. By assuming a homogeneous activity concentration for the scanning portion of volume in each fuel rod and a sufficiently large source-to-detector distance, the integration of eq. (3) for a fixed volume V_S gives the counting rate M [cps] by

$$M = pS\varepsilon' \int_{V_s} d\mathbf{r}_s \int_{A_d} d\Omega(\mathbf{r}_s, \mathbf{r}_d) \exp\left[-\sum_k \mu_k d_k(\mathbf{r}_s, \mathbf{r}_d)\right]. \quad (4)$$

As shown in Fig. 1, the scanning arrangement has a slit of 150 mm long and of 3 mm wide vertically in front of the collimator which is of 1220 mm long and of 30 mm wide horizontally. The HPGe detector views the fuel bundle through the slit at long distance compared with its diameter. Hence a 2-D approximation for the attenuation effect is adopted. A cartesian (x,y,z) coordinate system is taken as that the origin is at the rotational center on the plane of scan, z-axis is the rotation axis, x-axis the direction to the detector. Since the outer diameter of the bundle is smaller than 80 mm, the variation of solid angle for different source positions in the y-direction is within 0.2 %. Hence the variation of solid angle for different source positions is considered for the x-direction only. From eq. (4), the counting rate contributed by the i-th rod with the bundle rotated to angle θ is given by

$$M_{\theta,i} = pS_i\varepsilon' \int_z dz \int_{(x,y)_{\theta,i}} \Omega(x) \exp\{-\sum_k \mu_k d_k(x,y)\} dx\,dy = R_{\theta,i} S_i \quad (5)$$

and the response is

$$R_{\theta,i} = C \int_{(x,y)_{\theta,i}} \Omega(x) \exp\{-\sum_k \mu_k d_k(x,y)\} dx\,dy \quad (6)$$

where the constant is $C = p\varepsilon' \int_z dz$ and the detector efficiency is taken approximately as 15 % of which accurate value is not required since relative distribution of activity concentration is concerned in this study. The specification of the fuel bundle is listed in Table 2. The attenuation

Table 2. A Specification of the Fuel Bundle in This Study[19].

Length [mm]	960
Number of Element	36
• Standard core element	18
• Reduced core element	18
Meat	
• Composition	61.4 w/o U_3Si
	38.6 w/o Al
• Density(g/cc)	5.4
Element pitch [mm]	12
Central Rod	
• Material	Zircoly – 4
• Outer diameter [mm]	8.0

coefficients are taken from Hubbell and Seltzer[18]. The 8 cooling fins protuberant on the surface of cladding is simplified by increasing the annular thickness while keeping the volume equal. The Zr-4 central tie rod is taken into account but the Al spacer tubes surrounding Zr-4 rod are neglected due to the negligible attenuation. The path length d_k is obtained by approximating the γ-ray paths parallel to the collimator surface. The error between the approximated path length and the exact one is estimated less than 0.04 %, of which approximation gives an error in the attenuation effect within 0.02 % for the fuel meat where the attenuation is the strongest. The effect of self-attenuation and attenuation by a neighbour rod on the γ-ray path is shown in Fig. 3. The elements of response matrix for the rotation angle 0° are shown in Fig. 4.

2.3. The Solving Method

The direct methods solving eq. (2) by matrix inversion, have merits of conceptual clarity and analytical simplicity. Recently, the SVD(Singular Value Decomposition) method is known superior to other direct methods and hence is applied to

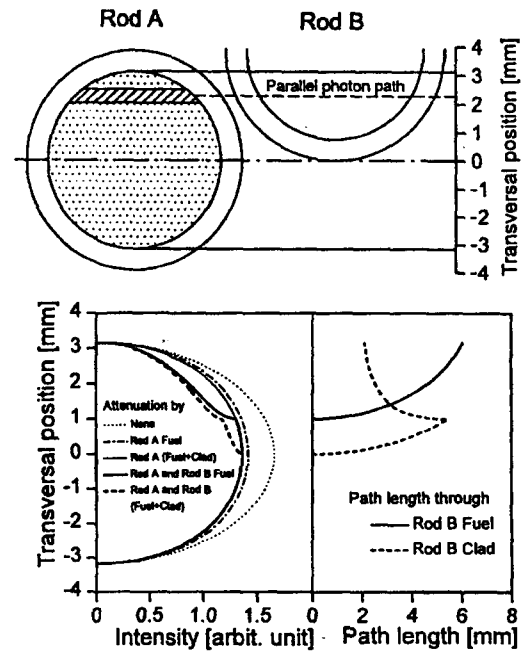

Fig. 3. The Intensity of γ-rays from the Transversal Section of Rod A. The Attenuation Effect by Rod B is Shown.

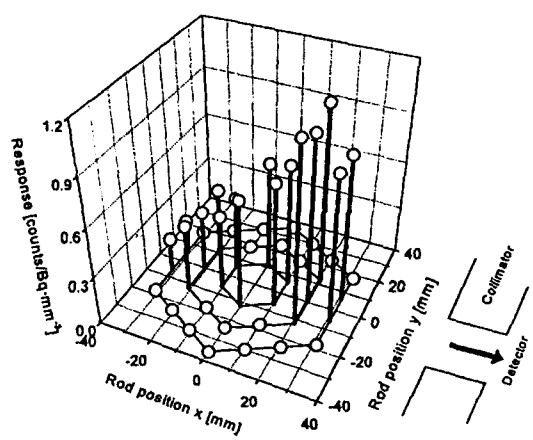

Fig. 4. Calculated Response from Each Rod by Setting the Scanning Angle of the Fuel Bundle at 0°.

medical imaging researches[20,21]. Therefore the applicability in this study is investigated for Gauss-Jordan method, ULD(Upper and Lower diagonal

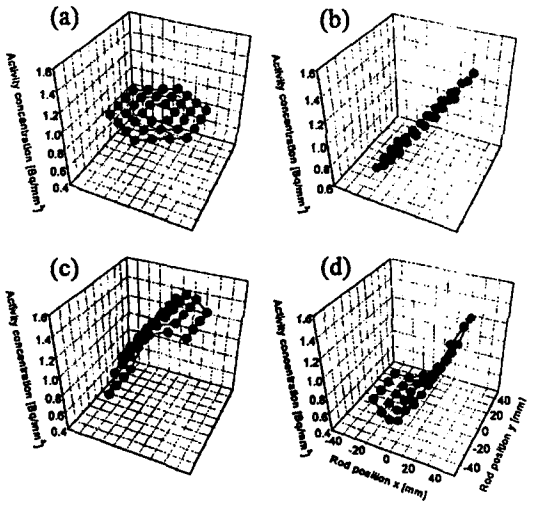

Fig. 5. Simulated Power Distributions with the Cross Sectional Shapes of Flat(a), Oblique(b), Negative(c) and Positive(d) Curvature.

matrix Decomposition) method and SVD method. The iterative methods have shown good stability for the inverse problem. The ILS(Iterative Least-Square) method, ML-EM (Maximum Likelihood-Expectation Maximizing) method and MEM(Maximum Entropy Method) are widely applied to various types of problems. Specificallly, ML-EM method and MEM are often used for the under-determined problem to obtain an estimated solution with probabilistic treatment due to insufficient number of measurements[22,23]. The ILS method is usually applied to the determined or the over-determined problem[24] and is known to be superior to others for noisy data[25]. The inverse problem in this work is a determined and ill-posed one. Hence a test of applicability is also performed for the ILS method.

Four hypothetical distributions for pin power are generated to test the performance of the solving method. The shapes of the distribution are 1) flat, 2) oblique, 3) of negative curvature and 4) of positive curvature on the cross sectional plane of scan. Fig. 5 shows the four virtual distributions used in the test examples. For the given response matrix, the accuracy of the numerical solution is hence estimated by comparing the solution of the inverse problem with the given power distribution. The example measurement data are generated in two sets of no error and of 5 % gaussian errors added for each predicted data by using the given response matrix.

All the results from the three direct methods gave accurate solutions within 0.01 % errors for the example data of adding no error, while the solutions for the data added by 5 % error showed instability including negative values. Hence, none of the direct methods turned out applicable to the present study of pin power distribution.

The ILS method obtains the vector S from minimizing the chi-square by iterative calculations,

$$\chi^2 = (\mathrm{M} - \mathbf{R}\mathrm{S})^T \mathbf{V}^{-1} (\mathrm{M} - \mathbf{R}\mathrm{S}) \tag{7}$$

where $\mathbf{V}$ is variance matrix. In this study, iterative relaxation method is chosen by considering the convergence speed[26], and the recurrence relation is used by

$$\mathrm{S}_{i_0}^{(n+1)} = \mathrm{S}_{i_0}^{(n)} + \delta \, \Delta \mathrm{S}_{i_0}^{(n)} \tag{8}$$

where

$$\Delta \mathrm{S}_{i_0}^{(n)} = \frac{\sum_\theta \frac{R_{\theta,i_0}}{\sigma_\theta^2} \left[N_\theta - \sum_i R_{\theta,i} \, S_i^{(n)} \right]}{\sum_\theta \frac{R_{\theta,i_0}^2}{\sigma_\theta^2}} \tag{9}$$

$$\delta = \frac{\sum_\theta \frac{1}{\sigma_\theta^2} \left(\sum_i R_{\theta,i} \Delta S_i^{(n)} \right) \left[N_\theta - \sum_i R_{\theta,i} \, S_i^{(n)} \right]}{\sum_\theta \frac{1}{\sigma_\theta^2} \left(\sum_i R_{\theta,i} \Delta S_i^{(n)} \right)^2} \tag{10}$$

and the superscript (n) is the iteration index. By this method, the same examples for the direct methods are solved. The reduced chi-square χ_ν^2

and the rms error σ_{RMS} are calculated at each iteration step to monitor the convergence and the accuracy by

$$\chi^{2\,(n)}_{\nu} = \frac{1}{36}\sum_{\theta}\frac{\left(M_\theta - \sum_i R_{\theta,i} S_i^{(n)}\right)^2}{\sigma_\theta^2} \qquad (11)$$

$$\sigma_{RMS} = \sqrt{\frac{1}{36}\sum_i \left(S_i^{(n)} - S_i^{exact}\right)^2} \qquad (12)$$

where $S^{(n)}$ is the numerical solution from the n-th iteration and S^{exact} is the exact solution given from the assumed power distribution. The solution values are expressed in ratio to the average power. For the error-free example data, the result of the ILS method shows a maximum of 8 % discrepancy while very accurate solution was obtained by the direct method. Fig. 6 shows the residual errors for the four examples. The result for the example data added by 5 % error is shown in Fig. 7. The stability of the solution is far better than that by direct methods. A typical variation of χ^2_ν and σ_{RMS} is shown in Fig. 8 where, as the iterations progress, the semi-convergence behavior[24] appears. Since an oscillation starts to diverge from the iteration of slower reduction in χ^2_ν, the calculation is stopped at the 4th iteration which is about the end period of rapid decrease in χ^2_ν.

3. Result and Discussion

Through a performance test, it has been proven that the stability of ILS method is better than the direct methods. The determined pin power distribution using the ILS method is shown in Fig. 9. The analysis method in this study could be evaluated accurately by scanning individual fuel pin after disassembling the bundle. Such an individual scan of fuel rod has once been applied to PWR spent fuel rods to determine burnup[27], this type of data however is not available yet for the fuels in

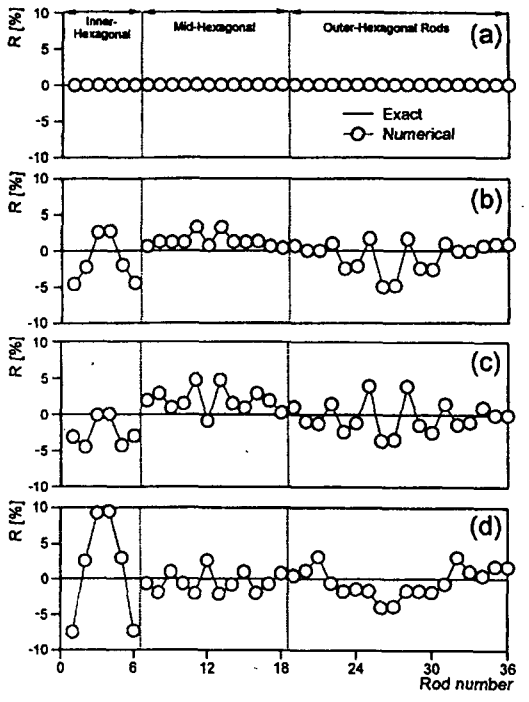

Fig. 6. Residual Errors of the Iterative Least-square Method for the Simulated Data of No Added Error. The Corresponding Simulated Power Shapes are of Flat(a), Oblique(b), Negative(c) and Positive(d) Curvatures, Respectively.

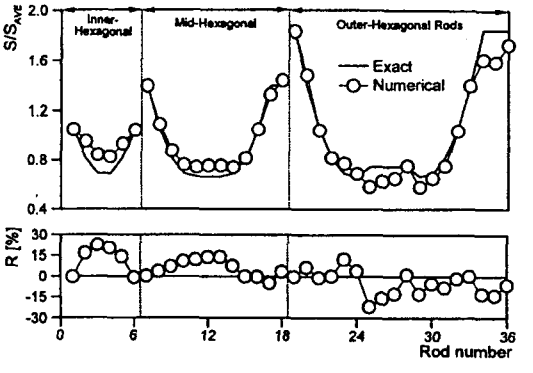

Fig. 7. The Power Distributions and the Residual Errors for the Case of Positive Curvature and the Simulated Data with 5 % Error Added are Obtained by the Iterative Least-square Method.

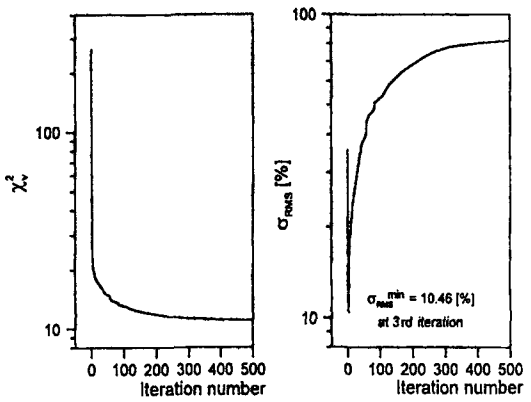

Fig. 8. The Variation x^2_ν and σ_{RMS} as Iterations Progress for the Case of Positive Curvature and the Simulated Data with 5 % Error Added.

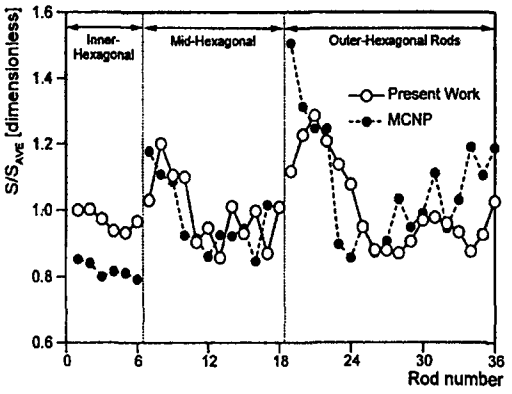

Fig. 9. Relative Pin Power Distribution Determined by the Iterative Least-square Method.

this study. Hence for an estimation of the accuracy, comparison with the core calculation[11] by the code MCNP is presented. The dashed line in Fig. 9 connects the result of MCNP calculation showing that the mutual differences are within ± 29 %. The comparison indicates a definite limitation of the present result.

Therefore the variables having sensitive influences on the accuracy of solution are seeked for. For that purpose, inverse problems with generated data of measurement are solved for the cases by varying the size of statistical error of detection, the size of rotation step and the collimator width. The problem solved by varying the size of the measurement error to 1 %, 5 %, and 10 % is plotted in Fig. 10. It is shown that reduction of the statistical error of measurement improves the accuracy. Then, an example data of 5 % error added is solved for the case of rotation step size reduced to 2°, where the number of measurements is increased by a factor of 5. The solution is shown in Fig. 11. Contrary to the expectation of improvement due to the abundant data from 180 measurements leading to an over-determined problem, the result shows no improvement. Since the required minimum number of measurements is given by[25],

$$n \approx \pi \frac{D}{d} \tag{13}$$

where D and d are the dimension of the object and the collimator width, respectively, the value n for this work is 8~9. Hence the present 36 measurements are sufficient and more measurements only by reducing rotational step size will give no appreciable improvements. The final example is generated for the case of reducing the collimator width from 30 mm to 10 mm. As shown in Fig. 12, the collimator width gives quite sensitive accuracy than the other variables. The width of 30 mm provides a view of 3 rods from the collimator, while a 10 mm width covers only one rod. This implies a 10 mm width is more appropriate to enhance the accuracy in distinguishing the power of one rod from those of neighbors.

The previous discussions draw a conclusion that the performance of the gamma-scanning and the

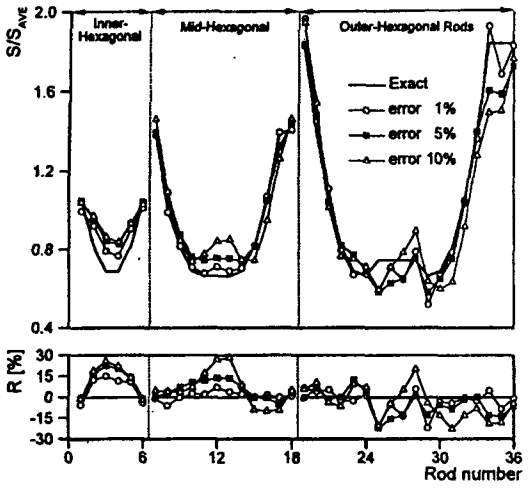

Fig. 10. Comparison of the Solutions Obtained by Varying the Error of Simulated Measurement.

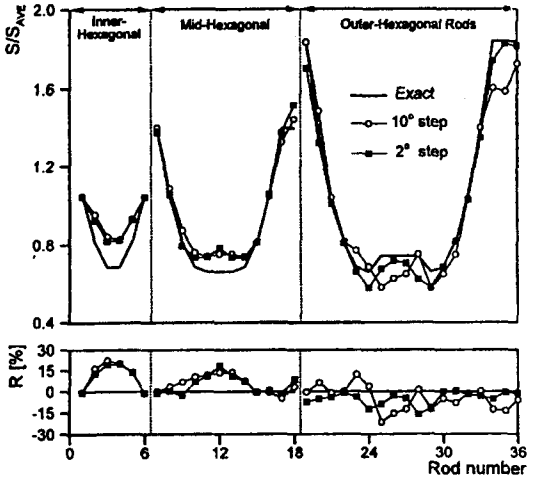

Fig. 11. Comparison of the Solutions Obtained by Varying the Rotational Step Size.

present analysis method is limited by the statistical error of measurement and the collimator width of the scanning device. While the accuracy can be improved by reducing the statistical error and the collimator width, the required time of detection is increased to reduce the statistical error of

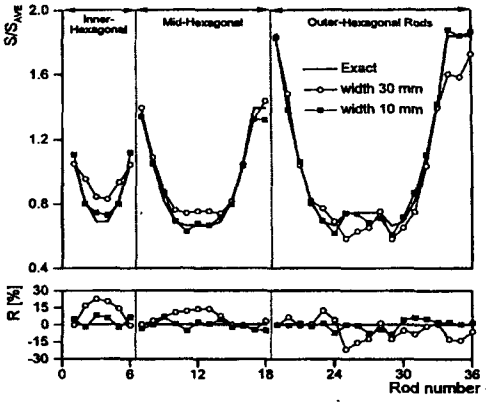

Fig. 12. Comparison of the Solutions Obtained by Varying the Collimator Width.

measurement by using smaller collimator width. Hence from a practical point of view, reducing the width of collimator to the size of viewing one rod will improve the accuracy significantly for the given amount of detection time.

4. Conclusions

In this study, the analysis of rotational gamma-scanning data with iterative least-square method is presented. Pin power distribution of fuel bundle irradiated in HANARO is determined and compared with the result of calculation by using the MCNP code. The improvement of accuracy by reducing the collimator width of the scanning device is predicted. To evaluate the power of present analyzing method in an accurate manner, new data measured with the reduced collimator width and also another data by scanning the individual rod are required and they remain for the suggested future work.

References

1. J.T. Dawson and G. Smith, *Nucl. Tech.*, **57**, 125 (1982)
2. G. Ducros, *Nucl. Tech.*, **68**, 370 (1984)

3. D.J. de Rosier and A. Klug, *Nature*, **217**, 130 (1968)
4. Z.H. Cho, *IEEE Trans. Nucl. Sci.*, **NS-21**, 44 (1974)
5. J.M. Hollis, J.E. Dorband and F. Yusef-Zadeh, *Astrophys. J.*, **386**, 293 (1992)
6. B.K. Barnes and J.R. Phillips, *Los Alamos Scientific Laboratory Report*, LA-4676 (1971)
7. B.K. Barnes, J.R. Phillips and M.L. Barnes, *Los Alamos Scientific Laboratory Report*, LA-UR-81-1662 (1981)
8. C. Niculae, T. Craciunescu and R. Dobrin, *Int. J. Ener. Res.*, **20**, 999 (1996)
9. D.F.G. Reher and B. Denecke, *Nucl. Instr. and Meth.*, **A312**, 273 (1992)
10. R.J. Estep, T.H. Prettyman and G.A. Sheppard, *Nucl. Sci. and Eng.*, **118**, 145 (1994)
11. B.J. Jun, Korea Atomic Energy Research Institute, private communications (1996)
12. J.D. Chen, D.G. Boase and R.B. Lypka, *Atomic Energy of Canada Limited Report*, AECL-5236 (1976)
13. Korea Atomic Energy Research Institute, *HANARO Safety Analysis Report*, Vol 2, KAERI/TR-710/96 (1996)
14. R.B. Firestone, V.S. Shirley, C.M. Baglin, S.Y.F. Chu and J. Zipkin, *Table of Isotopes* (1996)
15. *NUDAT Wallet wide format from NNDC, Feb 96.* (1996)
16. G.W. Phillips and K.W. Marlow, *Nucl. Instr. and Meth.*, **137**, 525 (1976)
17. S. Taczanowski, *Nucl. Instr. and Meth.*, **144**, 299 (1977)
18. J.H. Hubbell and S.M. Seltzer, NISTIR 5632 (1996)
19. Korea Atomic Energy Research Institute, *Complete Report for HANARO Work*, p.101, KAERI/PR-001/97 (1997)
20. T. Yuasa, M. Akiba, T. Takeda, M. Kazama, A. Hoshino, Y. Watanabe, K. Hyodo, F.A. Dilmanian, T. Akasuka and Y. Itai, *IEEE Trans. Nucl. Sci.*, **44**, 54 (1997)
21. G.L. Zeng and G.T. Gullberg, *IEEE Trans. Nucl. Sci.*, **44**, 107 (1997)
22. A.P. Dempster, N.M. Laird and D.B. Rubin, *J. Roy. Stat. Soc.*, **39**, 1 (1977)
23. E.T. Jaynes, *Phys. Rev.*, **106**, 620 (1957)
24. Å. Björck, *Numerical Methods for Least Square Problems*, SIAM (1996)
25. T.F. Budinger and G.T. Gullberg, *IEEE Trans. Nucl. Sci.*, **NS-21**, 2 (1974)
26. M. Goitein, *Nucl. Instr. and Meth.*, **101**, 509 (1972)
27. Y.-G. Lee, S.-H. Eom, K.-J. Park, K.-P. Hong, and S.-G. Ro, *J. Korean Nucl. Soc.*, **24**, 178 (1992)